Article

Ciprofloxacin-Loaded Composite Granules Enriched in Silver and Gallium Ions—Physicochemical Properties and Antimicrobial Activity

Kamil Pajor [1], Łukasz Pajchel [1] , Anna Zgadzaj [2], Paulina Kowalska [1], Anna Kowalczuk [3] and Joanna Kolmas [1,*

[1] Department of Analytical Chemistry, Faculty of Pharmacy, Medical University of Warsaw, ul. Banacha 1, 02-097 Warsaw, Poland

[2] Department of Environmental Health Sciences, Faculty of Pharmacy, Medical University of Warsaw, ul. Banacha 1, 02-097 Warsaw, Poland

[3] National Medicines Institute (NIL), Chelmska 30/34, 00-725 Warszawa, Poland

* Correspondence: joanna.kolmas@wum.edu.pl

Abstract: Various calcium phosphates (hydroxyapatite, α- and β-tricalcium phosphate, and brushite) containing silver or gallium ions were synthesized via standard methods and subjected to physico-chemical analysis by Fourier transform infrared spectroscopy (FT-IR), powder X-ray diffractometry (PXRD), and atomic absorption spectrometry (AAS). In the next step, the obtained calcium phosphate powders, sodium alginate, and chondroitin were used to produce composite granules. Ciprofloxacin, a broad-spectrum antibiotic that can be used in local delivery systems targeting bone tissue, was loaded into the granules. The release of silver and gallium ions as well as ciprofloxacin was then examined by inductively coupled plasma mass spectrometry (ICP-MS) and high-performance liquid chromatography (HPLC), respectively. The cytotoxicity of the granules was studied using a neutral red uptake (NRU) test and mouse embryonic fibroblasts. Moreover, preliminary antibacterial activity against *Staphylococcus aureus* and *Escherichia coli* was measured. The study showed that the type of calcium phosphates enriched in silver or gallium significantly affects the release profile of these ions. Biphasic calcium phosphates also have an impact on the morphology of the granules. Most of the granules turned out to be non-toxic to mammalian cells. Microbiological tests showed high antibacterial activity against both strains of bacteria.

Keywords: calcium phosphates; silver; gallium; ciprofloxacin; drug release

1. Introduction

Surgical site infection (SSI) is still a huge problem and a major challenge in orthopedic surgery. Conventional orthopedic implants are prone to bacterial adhesion and biofilm formation, making antibiotics less effective [1–3]. Orthopaedic SSI, which leads to a bone infection known as osteomyelitis, may be caused by many different strains of bacteria. The most common of these, i.e., *Staphylococcus aureus*, *Pseudomonas aeruginosa*, *Escherichia coli*, and *Acinetobacter baumanii*, can occur as resistant strains (e.g., methicillin-resistant *S. aureus*, MRSA), which hinder and prolong the treatment process and require a careful selection of antibiotics [1,4–7].

Ciprofloxacin, which belongs to the fluoroquinolone family, is one of the antibacterial drugs with favorable bactericidal and penetration effects on most bone infection pathogens [8–10]. Nevertheless, consistent increases in hospital-acquired infections caused by resistant strains of bacteria often reduce its effectiveness. According to the literature, the use of other antibacterial agents, such as silver and gallium ions, can help solve this problem [11,12].

Silver is well known as an antibacterial agent, used in the treatment of open wounds, burns, chronic ulcers, and on surfaces in hospitals to decrease nosocomial infections [13,14]. Silver exhibits a broad antimicrobial spectrum, including against various resistant strains, which is connected with the poor ability of microorganisms to develop immunity against silver [13,15]. The mechanism of action is mainly based on the interaction of silver with thiolic groups of proteins, where hydrogen atoms are exchanged for silver atoms. As a result, Ag-S bonding is formed, which causes the inactivation of bacteria proteins and, finally, cell death [15]. It is also worth noting that silver can enhance the antibacterial activity of antibiotics [14]. Unfortunately, higher concentrations of silver ions exhibit toxicity towards human cells, necessitating restricted therapeutic concentrations of silver.

The antibacterial mechanism of gallium action is known as "the Trojan horse strategy", which is strictly connected to its similarities with iron (such as the atomic radius, electronic configuration, and coordination chemistry). This results in gallium being actively transported into bacteria, where it replaces iron in various metabolic pathways, blocking them and impairing the functioning of bacterial cells [15–17]. Although its antibacterial activity is weaker, gallium is not as toxic as silver, and because of its different mechanisms of action, it can complement silver as an antibacterial agent.

In the treatment of bone infections, special attention must be paid to the route of administration of antibacterial agents. Antibiotics are typically administered intravenously or orally. Unfortunately, due to the low vascularity of bone tissue, it may lead to an increased risk of systemic adverse effects, their intensification, and the destruction of human natural microbiota because of the need for higher doses of drugs in order to obtain a therapeutic concentration in an infected area [18]. Therefore, the best solution to the aforementioned problem can be the direct delivery of antibiotics to bone tissue, as well as other antibacterial agents, in an attempt to widen the antibacterial spectrum of the implemented material [19].

Among biomaterials used in orthopedic surgery, calcium phosphates (CaPs) seem to be the best choice as a delivery system for antibacterial substances. CaPs (hydroxyapatite, $Ca_{10}(PO_4)_6(OH)_2$; α- or β-tricalcium phosphate: α- or β-$Ca_3(PO_4)_2$; and brushite $CaHPO_4 \cdot 2H_2O$) have become increasingly important as inorganic biomaterials, especially in orthopedics and dentistry, where they are used in fracture or bone defect treatments, total bone augmentation, spinal surgery, craniomaxillofacial reconstruction, and as dental implants and coatings for bone implants [20,21]. The interest in these materials results from their specific properties, especially their similarity to the mineral fraction of human bones and teeth [20,22]. CaPs exhibit bioactive behavior towards bone tissue, such as osteoconductivity and osteointegration, allowing the adhesion, proliferation, migration, and differentiation of bone cells, making these materials an excellent active scaffold for remodeling implanted bone [20,23,24]. Another crucial feature of CaPs, strictly connected to their potential use in delivery systems, is the ease with which they can adsorb drug substances, enabling them to be used as carriers for antibiotics or other antibacterial agents. Hydroxyapatite (HA) exhibits the highest similarity with the mineral fraction of bone tissue. However, tricalcium phosphate (TCP) and brushite (DCPD) are more soluble and biodegradable than HA [20,25]. By combining different CaPs and changing their ratios, biphasic or even multiphasic materials can be obtained, with adjustable properties, e.g., biomaterials with modified solubility, which facilitates a gradual release of antibacterial agents and drugs to the local environment [22,26,27].

To the best of our knowledge, there are few studies that focus on the development of materials that simultaneously deliver an antibiotic and ions with antibacterial properties [28,29]. Nevertheless, according to reports of a significant increase in the therapeutic effectiveness of antibiotics, while reducing the dose, such a solution seems to have great potential. The work in Ref. [30] also indicates a synergistic effect of these antibacterial agents and a less frequent occurrence of the problem of resistance.

The study presented in this work focused on the synthesis of different CaPs (HA, α-TCP, β-TCP, and brushite) doped with gallium or silver ions and then on the fabrication of porous composite granules containing these CaPs and loaded with ciprofloxacin. Physicochemical characterization of the obtained materials was performed using infrared spectroscopy, powder X-ray diffractometry, transmission and scanning electron microscopy, and atomic absorption spectrometry. The release kinetics of ciprofloxacin and gallium and silver ions were then explored. Preliminary biological studies were carried out, along with in vitro antibacterial activity against *Staphylococcus aureus* and *Escherichia coli*.

2. Materials and Methods

2.1. Synthesis of Silver- and Gallium-Containing Calcium Phosphate Powders

In this work, seven samples of different calcium phosphates enriched in silver or gallium ions were synthesized using the well-established wet method, which was described in detail in our previous work [31]. The powder materials obtained are listed in Table 1.

Table 1. List of all synthesized calcium phosphate powders with the estimated number of doped ions.

| Material	Comment	Nominal wt% of Doped Ion
Ag-HA	Silver-containing hydroxyapatite	0.22
Ag-aTCP	Silver-containing tricalcium phosphate α type	0.23
Ag-bTCP	Silver-containing tricalcium phosphate β type	0.23
Ag-DCPD	Silver-containing brushite	1.26
Ga-HA	Gallium-containing hydroxyapatite	3.35
Ga-aTCP	Gallium-containing tricalcium phosphate α type	3.61
Ga-bTCP	Gallium-containing tricalcium phosphate β type	3.61

The reagents used in the aforementioned procedure are presented below. Calcium nitrate tetrahydrate $Ca(NO_3)_2 \cdot 4H_2O$ (Sigma-Aldrich, Mumbai, India), ammonium dibasic phosphate $(NH_4)_2HPO_4$ (Chempur, Piekary Slaskie, Poland), gallium nitrate trihydrate $Ga(NO_3)_3 \cdot 3H_2O$ (Sigma-Aldrich, Burlington, MA, USA), and silver nitrate $AgNO_3$ (Avantor Performance Materials, Gliwice, Poland) were used as sources of calcium, phosphor, gallium, and silver, respectively. An adequate amount of $Ca(NO_3)_2 \cdot 4H_2O$ and $(NH_4)_2HPO_4$ was weighed out to obtain a specific molar ratio of (Ca + Ag)/P or (Ca + Ga)/P: 1.67 for hydroxyapatite, 1.5 for tricalcium phosphate, and 1.0 for brushite. An aqueous solution of ammonium dibasic phosphate was added dropwise into an aqueous solution of calcium nitrate tetrahydrate and one of the previously mentioned sources of gallium or silver, with gentle stirring. The mixture was then adjusted to a proper pH (10.0 for hydroxyapatite or tricalcium phosphate and 5.0 for brushite) and left under gentle stirring at a temperature of 60 °C for 2 h. Next, the precipitate was left aging for 24 h. Finally, the precipitates were washed, soaked several times with distilled water, and dried at 120 °C (HA and TCP) or 60 °C (DCPD) in air. In order to obtain TCPs from the synthesized powders, they were sintered at 700 °C for 8 h and then at 1050 °C for 8 h (β-TCP) or at 700 °C for 8 h and then at 1250 °C for 8 h (α-TCP).

2.2. Preparation of Biphasic Granules

The following reagents were used in order to fabricate biphasic granules: sodium alginate (Sigma Aldrich, Burlington, MA, USA), calcium chloride anhydrous $CaCl_2$ (Sigma-Aldrich, Shanghai, China), chondroitin sulfate sodium salt (TCI, Zwijndrecht, Belgium), and the previously synthesized powders: Ag-HA, Ag-aTCP, Ag-bTCP, Ag-DCPD, Ga-HA, Ga-aTCP, and Ga-bTCP.

Firstly, a 4% aqueous solution of sodium alginate was prepared at 40 °C, and an adequate amount of chondroitin sulfate sodium salt was added to obtain a 0.5% suspension. After this, seven types of granules were prepared by combining two different CaP powders: one doped with silver, and a second one doped with gallium ions; a total of 1.0 g of each

powder was added to 10 mL of the suspension and mixed thoroughly until dense, and a milky slurry was acquired. Approximately 0.2 g of ciprofloxacin hydrochloride (TCI, Tokyo, Japan) was then added to the slurry. At the same time, a cross-linking aqueous solution containing $CaCl_2$ (1.5%) was prepared. The slurry was added dropwise to the cross-linking solution with magnetic stirring, and granules were formed. These were left in the $CaCl_2$ solution for 20 min, then rinsed with distilled water several times, dried in air at room temperature, and lyophilized (see Figure 1). The obtained granules were covered with polycaprolactone (PCL) (Sigma-Aldrich, Gillingham, UK) by soaking them in a 7 % PCL chloroform solution. All the obtained granules are listed in Table 2.
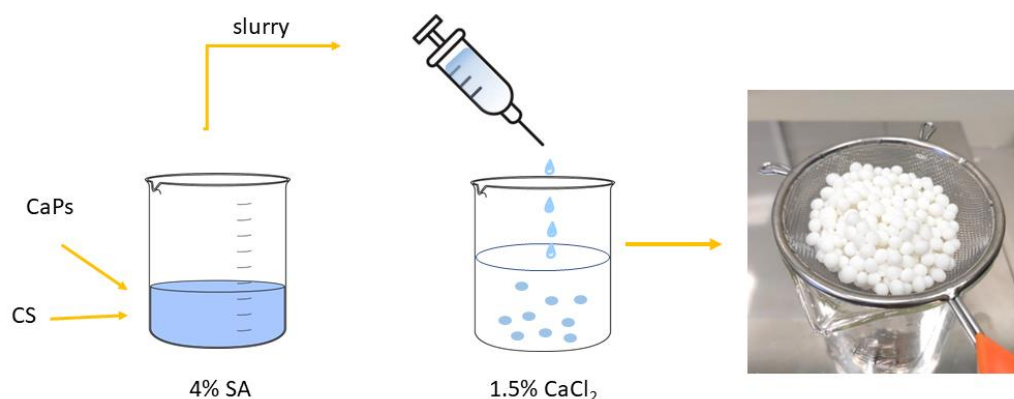
Figure 1. Scheme of composite granules preparation (CS—chondroitin sulfate, SA—sodium alginate, CaPs—different calcium phosphates).

Table 2. List of granules prepared of previously obtained CaP powders.

Standard Granules	Granules Layered with PCL	Silver Component	Gallium Component
G1	G1p	Ag-DCPD	Ga-HA
G2	G2p	Ag-DCPD	Ga-aTCP
G3	G3p	Ag-aTCP	Ga-bTCP
G4	G4p	Ag-HA	Ga-aTCP
G5	G5p	Ag-HA	Ga-bTCP
G6	G6p	Ag-bTCP	Ga-HA
G7	G7p	Ag-aTCP	Ga-HA

2.3. Physicochemical Analysis of CaP Powders

The chemical structure of all the obtained CaP powders was evaluated using Fourier transform infrared spectroscopy (FT-IR). The study was conducted using a Spectrum 1000 spectrometer (Perkin Elmer, Llantrisant, UK) using a standard KBr pellet technique. The measurements were performed with 30 scans and a 2 cm^{-1} resolution, over a range of 2000–400 cm^{-1}. Powder X-ray diffractometry (PXRD) was carried out to analyze the crystalline homogeneity. The study was performed using a PXRD diffractometer (Bruker D8 Advance, Bruker, Billerica, MA, USA) equipped with an LYNEXEYE position-sensitive detector and with Cu-Kα radiation (λ = 0.15418 nm). The data were collected using Bragg–Brentano (θ/θ) horizontal geometry in flat reflection mode (between 20° and 45°) (2θ) in a continuous scan, and 0.08° steps and 2 s/step were used, with a total time equal to 384 s/step. Phases for obtained diffractograms were determined by comparing them with adequate standard patterns (JCPDS 09-0077 for DCPD, JCPDS 09-0432 for HA, JCPDS 09-0169 for β-TCP, and JCPDS 09–0348 for α-TCP).

FT-IR spectra and PXRD diffractograms were then processed in GRAM/AI 8.0 software (Thermo Scientific, Burlington, ON, USA) and KaleidaGraph 3.5 Software (Synergy Software, Reading, PA, USA).

Atomic absorption spectrometry (AAS) was conducted to evaluate the content of Ag^+ and Ga^{3+} in the synthesized CaP powders. The study was carried out on an AAS spectrometer (ANALYST 400, Perkin Elmer, Llantrisant, UK), with detection at a wavelength of $\lambda = 287.42$ nm and $\lambda = 328.07$ nm, for gallium and silver, respectively. The samples were prepared by dissolving the powder in super-pure 63% nitric acid and diluting the obtained solution with distilled water. The calibration curves were prepared by dissolving an adequate amount of calibration standard in distilled water—$AgNO_3$ (Avantor Performance Materials, Gliwice, Poland) and $Ga(NO_3)_3 \cdot 3H_2O$ (Sigma-Aldrich, Burlington, MA, USA), for silver and gallium, respectively—and then preparing the dilution series in distilled water.

2.4. Physicochemical Analysis of Granules

Scanning electron microscopy (SEM) using a JSM 6390 LV SEM microscope (JEOL, Tokyo, Japan) (at 20 or 30 kV accelerating voltage) was conducted to examine the morphology of the obtained granules. Before the experiments, the granules were covered with a gold layer in a vacuum chamber, and images were taken of the outer and inner surfaces (after the cross-section).

The release study was performed for all granules containing ciprofloxacin. Therefore, 0.5 g of granules was put into a conical tube, to which 50 mL of phosphate-buffered saline (PBS) (pH = 7.4) was added. The tubes were then placed in a water bath at 37 °C under continuous stirring. The release studies of ions (gallium and silver) and ciprofloxacin were carried out for four weeks. Sample aliquots were collected after 1 h, 2 h, 3 h, 6 h, 12 h, 24 h, 48 h, 5 days, 7 days, 14 days, and 28 days. After the collection of the samples, the tubes were replenished with PBS as per the initial volume.

In order to determine the amount of silver and gallium ions released from the granules, inductively coupled plasma mass spectrometry (ICP-MS, Agilent Technologies 7800, Santa Clara, CA, USA) was used. Samples and a dilution series for calibration curves were prepared in the same manner as previously, with a change of solvent from distilled water to PBS.

The amount of ciprofloxacin released was evaluated using a reverse-phase HPLC method. An HPLC instrument was used, consisting of a column (Varian RP-18, 250×4.6 mm), thermostat (Shimadzu CTO-10ASVP, Shimadzu, Tokyo, Japan), pump (Varian Prostar 210), injection loop (20 mL Rheodyne), and UV-Vis detector (Varian Prostar 325). The mobile phase was composed of acetonitrile and phosphate buffer (pH = 3.0; 20:80), with detection at a wavelength of $\lambda = 278$ nm.

2.5. In Vitro Cytotoxicity Study

The neutral red uptake assay was conducted in accordance with ISO 10993, Annex A [32,33], with BALB/c 3T3 mouse embryonic fibroblasts (American Type Culture Collection). Quantitative estimation of the cell viability was based on their neutral red uptake compared to the untreated culture. Cells were seeded in 96-well microplates (15,000 cells/100 µL) in Dulbecco's Modified Eagle Medium (Lonza), supplemented with 10% of calf bovine serum, 100 IU/mL penicillin, and 0.1 mg/mL streptomycin, and incubated for 24 h (5% CO_2, 37 °C, >90% humidity). After that, each well was examined to ensure that the cells formed a confluent monolayer. The culture medium was replaced by the extracts. Extracts were obtained by the preincubation of the materials in a culture medium (100 mg/mL) with a 5% serum concentration, at 37 °C for 24 h and sterilized by filtration. Cells were treated with a twofold dilution series of the extracts for 24 h at 540 nm. As the reference materials, polyethylene film and latex were used (non-cytotoxic and highly cytotoxic, respectively). The cell viability was calculated by comparing OD540 then the treatment medium was removed. The cultures were washed with PBS and treated with medium containing the dye for 2 h. The medium was discarded, and the cells were washed with PBS and treated with an ethanol and acetic acid water solution (desorbing fixative). The color of each well was evaluated colorimetrically, results were compared with

the untreated control. Samples were classified as cytotoxic if they reduced cell survival to below 70%. If the BALB/c 3T3 fibroblasts retained a viability of at least 70% across the full range of tested dilutions, they were considered to be non-cytotoxic.

2.6. Microbiological Activity Studies

The antibacterial activity of the synthesized granules was assessed against Gram-negative *E. coli* bacteria (ATCC 25922) and Gram-positive *S. aureus* bacteria (ATCC 6438), according to a methodology previously reported in [34], with 0.5 McFarland standard microbial cultures. Bacterial strains cultured on MacConkey and Columbia agar (Biocorp, Warsaw, Poland) were transported to Tryptic soy broth medium (Merck, Burlington, MA, USA) and incubated for 24 h at 37 °C, after which the density of the bacterial suspension was measured using a densitometer (Biomerieux, Marcy-l'Étoile, France) and then diluted to a density with an order of magnitude equal to 10^6 CFU/mL. Next, 50 mg of each type of granule produced was placed in 5 mL of Tryptic soy broth medium, and the bacterial suspensions prepared earlier were added. The mixture was incubated for 24 h at 37 °C, after which the bacterial colonies were counted using a Scan300 counter (Interscience, Saint Nom la Bretêche, France). As a positive control (C+), free microbial culture was assessed at the same time intervals. The measurements were repeated three times. The data are presented as mean ± SD.

3. Results

3.1. Characterization of Synthesized Powders

In the first step, the selected calcium phosphates containing silver or gallium ions were synthesized (see Table 1). For comparison, their unsubstituted counterparts—hydroxyapatite (HA), α- and β- tricalcium phosphates (aTCP and bTCP, respectively), and dicalcium phosphate dihydrate (DCPD)—were prepared using the same methods.

It should be noted that while there are many papers on substituted hydroxyapatite in the available literature, substitutions with silver and gallium ions in other calcium phosphates (brushite, α -TCP, and β -TCP) are described in only a few papers [28,31,34–37].

Figure 2A,B show the FT-IR spectra in the most informative range: 2000–400 cm^{-1}. The spectra of the Ag-HA and Ga-HA samples were similar and had a dominant band at approximately 1110–955 cm^{-1} and bands at approximately 603 and 565 cm^{-1}, corresponding to the vibrations of $\nu_1 + \nu_3$ and ν_4 of the apatite phosphates, respectively. Both spectra exhibited a band at approximately 630 cm^{-1}, originating from the liberational vibrations of the structural OH groups of HA [35,38].

The spectra of the Ag-aTCP and Ga-aTCP samples were characterized by very wide and poorly separated bands, similar to the spectra of unsubstituted α-TCP (as evidenced in the literature and Figure S1 in Supplementary Materials) [39–41]. It should be noted that the spectra were very complex and barely identifiable, which is consistent with theoretical data showing that the α-TCP spectrum can contain up to 216 phosphate bands (24 distinct bands in the case of ν_1; 48 distinct bands for ν_2; and 72 bands each for ν_3 and ν_4) [40]. In addition, it should be noted that the Ag-aTCP spectrum showed a narrow band at approximately 725 cm^{-1}, which is characteristic of pyrophosphates formed during the thermal treatment of calcium phosphates [41–43]. This band was also present in the spectra of samples synthesized at high temperatures: Ag-bTCP and Ga-bTCP.
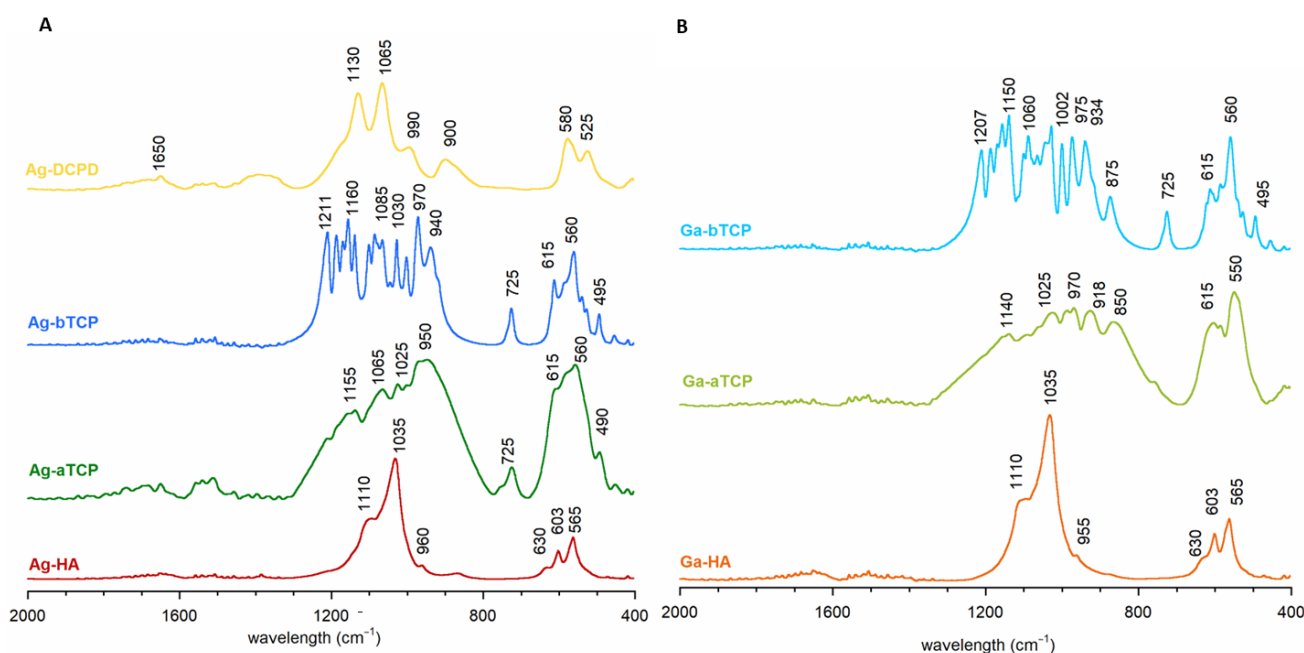
Figure 2. FT-IR spectra of the obtained calcium phosphates: (**A**) enriched with silver ion, (**B**) enriched with gallium ion.

As for the spectra of Ag-bTCP and Ga-bTCP samples (Figure 2), in the ν_1 and ν_3 vibration region, they contained narrow, well-separated bands, which is characteristic of β-TCP [39,44]. In turn, the ν_4 region contained two major bands (at approximately 615 and 550 cm^{-1}), confirming the β-TCP structure of these materials (see Figure S1).

The representative spectrum of brushite enriched with silver ions (Ag-DCPD) is presented in Figure 2A. The dominant features here are ν_3 phosphate bands at approximately 1130 and 1065 cm^{-1}, as well as ν_1 bands at approximately 990 cm^{-1}. The wide band at 900 cm^{-1} proves the presence of P-OH groups, characteristic of the structure of brushite (Figure S1 in Supplementary Materials). In the ν_4 region, two typical DCPD bands can be seen at 580 and 525 cm^{-1} [45,46].

The PXRD diffractograms of the obtained powders are shown in Figure 3A,B. For comparison, the patterns of the unsubstituted powders are summarized in Figure S2 in Supplementary Materials. All reflections on the Ag-HA and Ga-HA diffractograms were indexed to hydroxyapatite (JCPDS 09-432). The reflections were wide, especially for the Ga-HA sample, which is typical of nanocrystalline samples.

In turn, the PXRD pattern of the Ga-aTCP sample exhibited narrow, sharp reflections only from the α-TCP crystalline structure (JCPDS 09-348). The diffractogram of the Ag-aTCP sample contained additional reflections at approximately 27.0 and 27.9°, attributable to calcium pyrophosphate, in accordance with the presented FT-IR tests.

The Ag-bTCP and Ga-bTCP samples were not homogeneous and, like Ag-aTCP, contained calcium pyrophosphate. The diffractogram for the Ag-DCPD sample showed the presence of only one crystalline phase; all reflections originated from the brushite structure (JCPDS 09-077).

For all the obtained powders, the content of silver and gallium was examined by AAS spectrometry. It turned out that the ions were introduced with a fairly good yield from 66 to 97%. The concentration of silver decreased in the following order: Ag-DCPD (1.06 ± 0.03 wt.%); Ag-bTCP (0.20 ± 0.02 wt.%); Ag-aTCP (0.18 ± 0.03 wt.%); and Ag-HA (0.15 ± 0.02 wt.%).
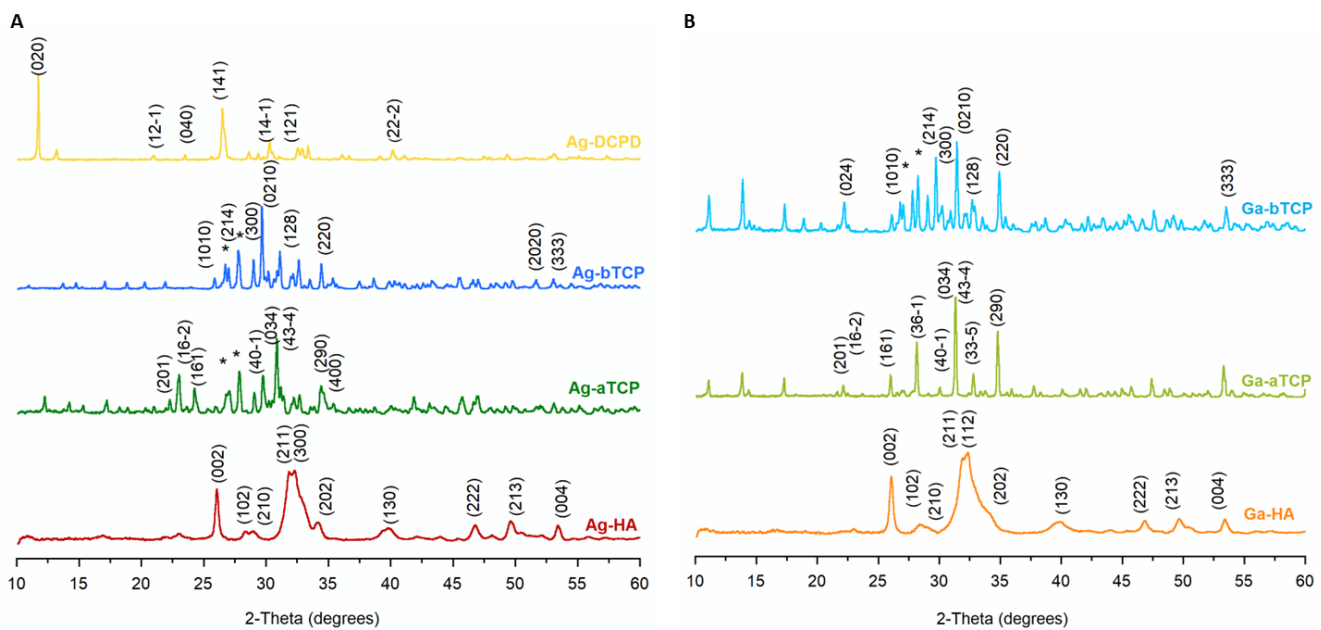
Figure 3. PXRD diffractograms of the obtained calcium phosphates: (**A**) enriched with silver ion, (**B**) enriched with gallium ion (*-calcium pyrophosphate).

Ga-aTCP and Ga-bTCP were synthesized at high temperatures. The amount of gallium was approximately 3.50 ± 0.02 and 3.52 ± 0.03 wt.%, and the substitution efficiency was the highest (97%). In turn, the gallium concentration in the Ga-HA sample amounted to 2.21 ± 0.02 wt.%, which was 66% of the nominal value.

The above physicochemical tests of the obtained CaPs powders allowed us to confirm their identity and the degree of substitution with foreign ions, i.e., silver and gallium.

3.2. Morphology of the Synthetic Granules

The next step was to obtain composite granules containing alginate, chondroitin sulfate, and two different calcium phosphates enriched with silver and gallium ions. In this way, seven types of granules were obtained (see Table 2).

According to literature reports, bone substitute materials are often prepared in the form of granules or microgranules [47,48]. This form is beneficial in the case of filling small bone defects. Moreover, by filling the 3D space, the materials form intra-granular pores between the granules, thus contributing to better vascularization and facilitated adhesion of bone cells.

Representative SEM photos of each granule type are shown in Figure 4.

Figure 4A shows a granule in its entirety. It can be seen that it has a regular, spherical shape, quite a rough surface, and an average diameter of 3–4 mm. The images that follow (Figure 4B–H) depict cross-sections of the granules. G1 and G2 granules are characterized by the most compact structure, with the least developed surface. In both of these, single clusters of crystals are visible, with elongated shapes, typical of brushite (DCPD). The cross-sections with the highest porosity and the least homogeneous structure belong to the G3, G4, and G7 samples. The G5 sample appears to be the most homogeneous, with regular microporosity.

All types of granules were also prepared by covering them with an additional layer of PCL. This treatment did not significantly affect the morphology of the surface or the interior of the granules (data not shown).
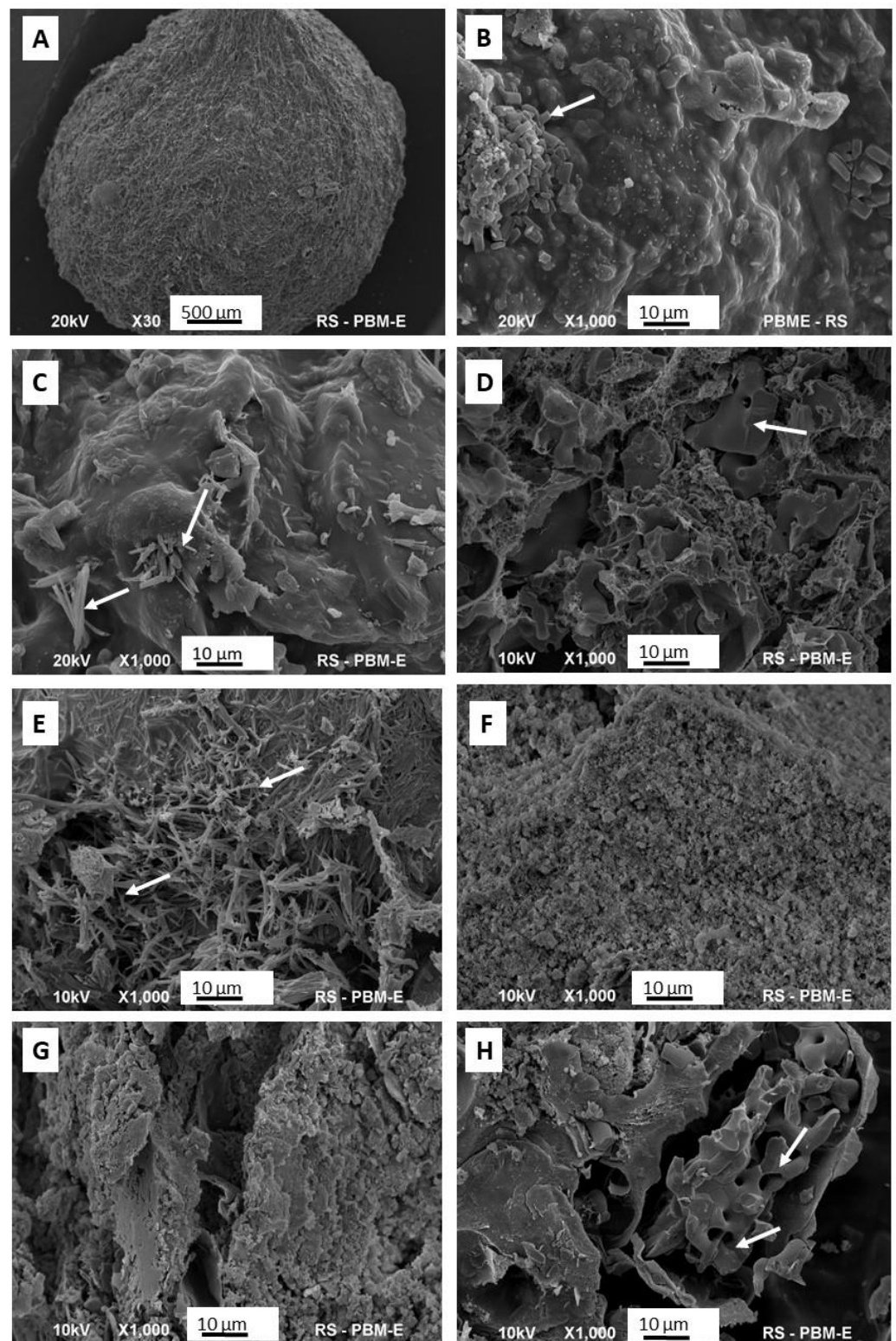
Figure 4. SEM representative images of the granules: (**A**) the outer surface of the granule; (**B–H**) internal cross-sections of granules G1–G7. The arrows indicate the crystals of calcium phosphates.

3.3. Ion Release Studies

The obtained composite granules were tested for the release of silver and gallium ions. Figure 5 shows the silver release curves for standard and polycaprolactone-coated granules (A and B, respectively). Figure 5A clearly shows that the greatest amount of released silver could be observed for samples containing Ag-DCPD powder (curves G1 and G2). In granules containing tricalcium phosphates (i.e., Ag-aTCP and Ag-bTCP), no silver release was observed throughout the entire study period (samples G3 and G6; results not shown), or the release of silver was significantly delayed. In the case of sample G7, the first concentration of released silver was recorded on the fifth day.
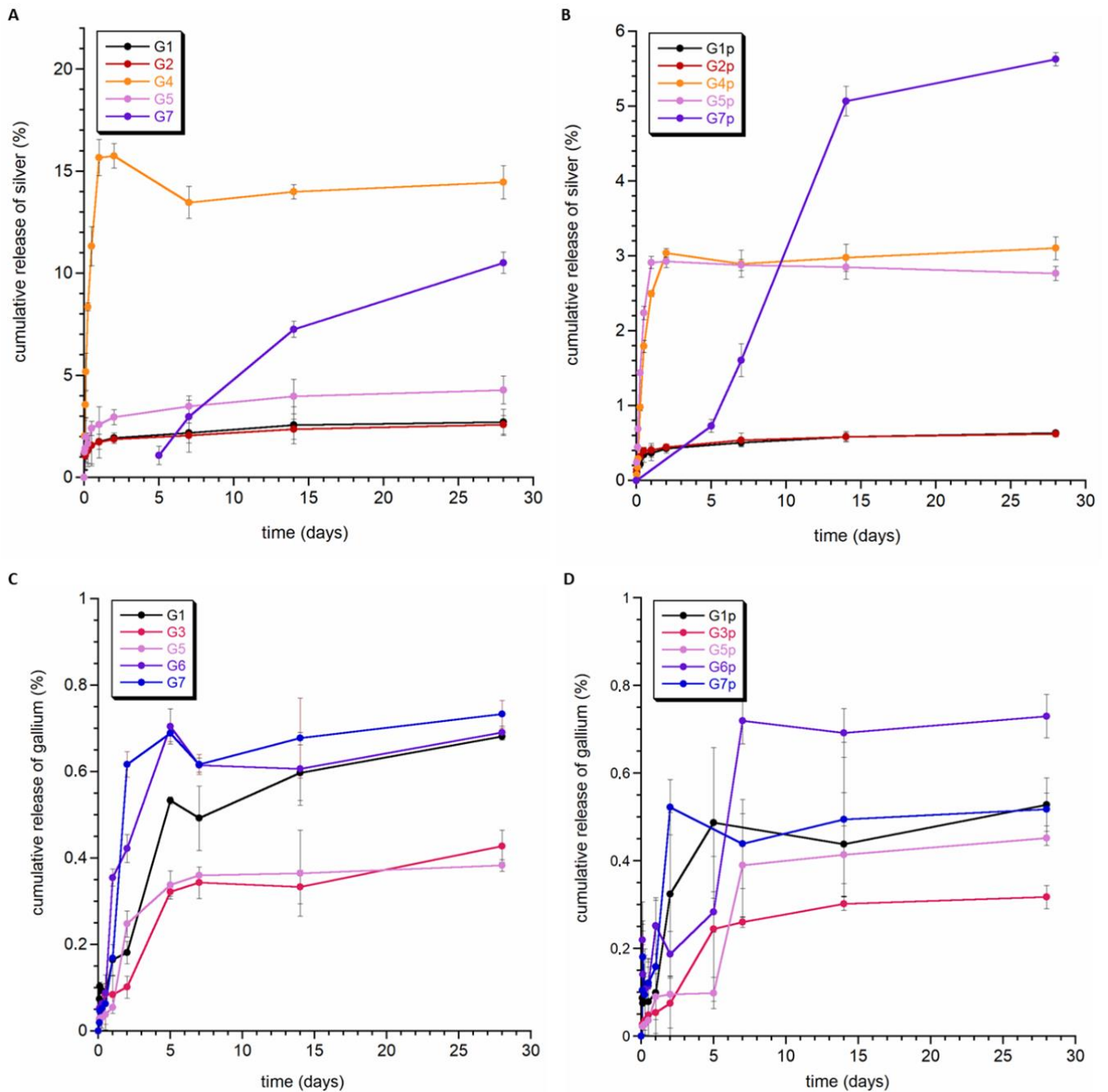

Figure 5. Release profiles of silver (**A**,**B**) and gallium ions (**C**,**D**) from the granules.

It is also worth noting that the amount of silver released from the G1 and G2 granules was similar, so it can be assumed that the composition of these granules and their morphology did not have a significant impact on the release of silver ions, and the main factor determining the kinetics of release was the type of CaP, to which silver ions were introduced.

The granules containing silver ions in hydroxyapatite (G4 and G5) were characterized by different kinetics of Ag^+ release to those of the G1 and G2 granules. Silver ions were released during the first 50 h, and then, a plateau could be observed in the curve. Considering the fact that hydroxyapatite is characterized by lower solubility than brushite, it can be assumed that the released silver ions mainly came from the surface of apatite crystals. This is also supported by the low degree of Ag^+ release (the remaining amount was not released during the experiment). It is also worth noting that sample G5 had the smallest amount of released silver, most likely due to the different morphology of the granule interior.

Covering the composite samples with an additional layer of PCL polymer (Figure 5B) did not cause any significant differences in the silver ion release profile. On the other hand, in all but one of the samples (i.e., not G5), the total amount of released ions decreased significantly (even almost five-fold). As with granules without PCL, no release or a delayed release was observed in samples containing Ag-TCP (sample G7—first measurements on the fifth day of the experiment).

Figure 5C,D show the gallium ion release profiles for granules with and without the cover of PCL. Of particular note is the fact that, despite the higher content of gallium than silver in the samples, a significantly lower degree of release was recorded. There was also a smaller difference between the release of gallium from the PCL and non-PCL samples. Samples G2 and G4 showed a trace release of gallium ions (data not shown). In both samples, the gallium ions were substituted into α-TCP crystals. The G1, G3, G5, G6, and G7 granules released a similar amount of gallium ions at a similar rate (see Figure 5C).

Summarizing the obtained results, it can be stated that the release of both silver and gallium ions is very slow. During the time under study (28 days), the percentage of released silver did not exceed 20%, and gallium was even lower and did not reach 1%. We can therefore assume that the obtained materials are stable during this time, and the release will proceed with the degradation of the obtained granules. It should be noted that we presented similar research on the release of silver and gallium ions from hydroxyapatite-containing granules in Ref. [49], and we also demonstrated a slow release of these ions there. The results of ion release from granules containing non-apatite silver and gallium sources are shown here for the first time.

3.4. Ciprofloxacin Release

Figure 6 shows the release profile of ciprofloxacin from granules G1–G7 (without PCL coating) and G1p–G7p (with PCL coating). Generally, the percentage of ciprofloxacin released in vitro at pH = 7.4 ranged between 38% and 55%. For each type of granule, the release profile of ciprofloxacin was characterized by a slight burst release in the first few hours (see Figure 6B,D). It can be assumed that the type of material does not have a significant impact on the drug release profile, although coverage of PCL granules seemed to weaken the release of the drug during the first few hours in some samples (G1p, G4p, G5p, and G7p). At the same time, it could also be seen that the total amount of released ciprofloxacin was slightly lower for the PCL-coated samples than for the standard granules.

In Figure 6, instead of a plateau, a slight tendency towards a downward curve can be observed (see Figure 5A,B, G5 and G7 curves). This may be related to the high affinity of calcium phosphates to the adsorption of drug molecules. It is worth noting that the ease of adsorption of molecules and ions depends on many factors, including the chemical properties of the adsorbed molecules and their size, but also the surface properties of calcium phosphate (including their surface area, porosity, and particle morphology). Each type of granule contained two different calcium phosphates; however, in each case, one of them was hydroxyapatite enriched with silver or gallium ions. Our research and

the available literature show that substitution with gallium and silver ions affects the morphology and size of crystals [31,50]. Significant reduction in the size of crystals and their strong tendency to form agglomerates occurs for apatite samples containing gallium ions. The powders consist of very fine plate-like crystals in the order of a few nanometers in size. This makes them characterized by a very large specific surface area and, thus, high susceptibility to adsorption. Therefore, it can be assumed that the downward slope of the curves is related to the re-adsorption of the drug on the surface of calcium phosphate, in particular, nanocrystalline hydroxyapatite.
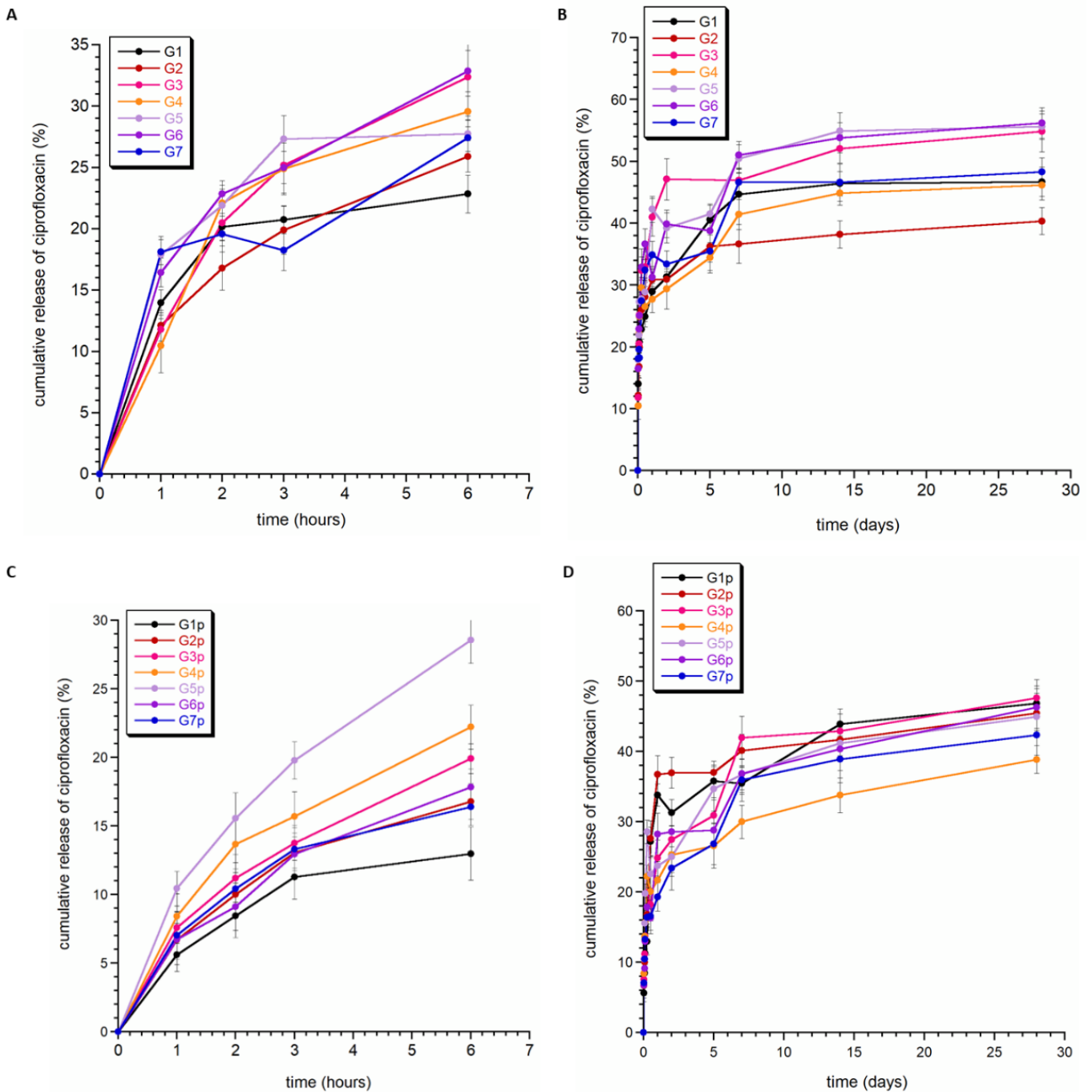
Figure 6. Release profiles of ciprofloxacin from the granules without PCL (**A**,**B**) and the granules with PCL (**C**,**D**).

The semi-empirical Korsmeyer–Peppas model was used to evaluate the mechanism of ciprofloxacin release from the obtained composites. This model was chosen because it is dedicated to the description of drug release from polymer systems and typical hydrogels. Moreover, the use of this model is possible when the amount of released drug substance does not exceed 80% [51,52].

The model is described by the following formula:

$$X\% = kt^n, \text{ where}$$

X% is the fraction (in %) of the dissolved drug at a given time t;
K is the constant describing the features of the structure and geometry of the matrix;
N is a parameter indicating the release mechanism [53].

Figure 6B,D show that the percentage of ciprofloxacin released did not exceed 60%. The fitting parameters are presented in Table 3. The correlation coefficient (R^2) in all fittings was quite high and ranged between 0.9239–0.9979. The n parameter describing the drug release mechanism, for all analyzed fittings, was in the range of 0–0.45. In the Korsmeyer–Peppas model, for $n \leq 0.43$, drug release kinetics occur according to Fickian diffusion from polydispersive systems (see Figure S4A,B in Supplementary Materials) [50]. Thus, we can conclude that the obtained materials release the drug similarly to typical hydrogels: quite quickly and with non-zero kinetics.

Table 3. Fitting parameters for ciprofloxacin release from granules (k—constant; n—parameter of release mechanism; R^2—correlation coefficient).

Sample	k/min^{-n}	n	R^2
G1	17.0 ± 1.1	0.17 ± 0.01	0.9791
G2	11.5 ± 2.1	0.23 ± 0.03	0.9351
G3	17.9 ± 1.4	0.13 ± 0.02	0.9979
G4	21.8 ± 2.4	0.15 ± 0.02	0.9238
G5	11.1 ± 1.2	0.16 ± 0.01	0.9331
G6	11.0 ± 1.1	0.23 ± 0.02	0.9791
G7	17.7 ± 1.8	0.15 ± 0.02	0.9324
G1p	12.7 ± 0.9	0.17 ± 0.02	0.9683
G2p	21.0 ± 1.5	0.16 ± 0.02	0.9655
G3p	14.9 ± 1.5	0.15 ± 0.02	0.9494
G4p	21.4 ± 1.7	0.15 ± 0.02	0.9555
G5p	10.6 ± 1.2	0.23 ± 0.02	0.9711
G6p	18.9 ± 1.8	0.15 ± 0.02	0.9384
G7p	9.4 ± 0.2	0.24 ± 0.02	0.9855

3.5. Cytotoxicity Studies

The viability of the BALB/c 3T3 cells did not fall below 70%, in comparison to the untreated control, in most samples. Therefore, all these materials were classified as non-cytotoxic in the neutral red uptake assay (see Table 4). Only G1, G2, and Ag-DCPD powder (all samples containing brushite doped with silver ions) decreased the viability of 3T3 cells to less than 70% after exposure to the undiluted extracts (100 mg/mL), and these were classified as cytotoxic. However, in the first dilutions of the twofold dilution series, none of the samples negatively affected the cell culture condition, i.e., the cell viability did not differ from the untreated control (see Figure 6).

Table 4. Results of the neutral red uptake test for the highest concentrations of tested extracts (100 mg/mL) in comparison to the untreated control.

Sample	Cell Viability ± SD [%]	IC50 [mg/mL]	Classification
Pure HA	101 ± 2	N	Non-cytotoxic
Ag-HA	102 ± 4	N	Non-cytotoxic
Ga-HA	94 ± 4	N	Non-cytotoxic
Pure β-TCP	105 ± 2	N	Non-cytotoxic
Ag-bTCP	98 ± 3	N	Non-cytotoxic
Ga-bTCP	114 ± 1	N	Non-cytotoxic
Pure α-TCP	101 ± 3	N	Non-cytotoxic
Ag-aTCP	106 ± 3	N	Non-cytotoxic
Ga-bTCP	99 ± 1	N	Non-cytotoxic
Pure DCPD	111 ± 6	N	Non-cytotoxic
Ag-DCPD	<u>21 ± 10</u>	<u>83</u>	Cytotoxic
G1	<u>10 ± 7</u>	<u>76</u>	Cytotoxic
G2	<u>44 ± 4</u>	<u>94</u>	Cytotoxic
G3	99 ± 3	N	Non-cytotoxic
G4	87 ± 4	N	Non-cytotoxic
G5	100 ± 4	N	Non-cytotoxic
G6	85 ± 4	N	Non-cytotoxic
G7	99 ± 3	N	Non-cytotoxic
LT	<u>0 ± 0</u>	<u>≤10</u>	Cytotoxic
PE	102 ± 7	N	Non-cytotoxic

LT—latex, reference cytotoxic material. PE—polyethylene foil, reference non-cytotoxic material. N—calculation was not possible due to the lack of cytotoxicity in the whole range of tested concentrations. Results with cell viability decreased under 70% are underlined.

The obtained results are very promising. In the case of hydroxyapatite and tricalcium phosphate, they show that the amount of silver and gallium introduced did not cause a toxic effect on fibroblasts. Our previous studies on silver-containing hydroxyapatite [31] showed that a higher amount of silver in the HA powder obtained by the same method is cytotoxic, as is the gallium-containing hydroxyapatite obtained by the dry method (unpublished data). In turn, attention should be paid to the toxicity of the Ag-DCPD material and granules containing this material. Further research on the optimal concentration of silver is required in order to obtain a material that is non-toxic to mammalian cells.

3.6. Antibacterial Activity

The results for the test of antibacterial activity against *S. aureus* and *E. coli* for the synthesized granules are presented in Tables 5 and 6. It can be seen that biphasic granules containing ciprofloxacin (both without cover and covered with polycaprolactone) exhibited antibacterial activity against both strains of bacteria, reaching a 6-logarithmic reduction in bacterial growth in most samples. All types of granules reduced the growth of Gram-negative *E. coli* bacteria entirely. On the other hand, in the case of Gram-positive *S. aureus* bacteria, diminished antibacterial activity could be observed for G1 and G2 granules (with and without PCL), which were the only granules composed of brushite. The full impact of the aforementioned granules on the bacterial growth of *S. aureus* is shown in Table 6. It should be mentioned that the antibacterial activity of granules containing brushite decreased over time (with a similar observation recorded for *E. coli*).

Table 5. Bacterial growth of *S. aureus* and *E. coli* in medium containing examined samples after 24 h of incubation.

Type of Granules	Bacterial Growth [CFU/mL]	
	Staphylococcus aureus	*Escherichia coli*
G1	1.25×10^3	0
G2	1×10^2	0
G3	5×10^1	0
G4	5×10^1	0
G5	5×10^1	0
G6	5×10^1	0
G7	0	0
G1p	1.5×10^3	0
G2p	2.75×10^3	0
G3p	0	0
G4p	0	0
G5p	0	0
G6p	0	0
G7p	0	0

The average initial bacterial concentration for *S. aureus* was equal to 5×10^6 CFU/mL. The average initial bacterial concentration for *E. coli* was equal to 4.75×10^6 CFU/mL.

Table 6. Bacterial growth of *S. aureus* in a medium containing selected examined samples after 24 h of incubation in three repetitions with weekly intervals.

Type of Granules	Bacterial Growth—*Staphylococcus aureus* [CFU/mL]		
	1st Week	2nd Week	3rd Week
G1	1.25×10^3	2.61×10^4	1.55×10^5
G1p	1.5×10^3	1.65×10^3	4.96×10^5
G2	1×10^2	1.45×10^3	2.51×10^5
G2p	2.75×10^3	4.68×10^4	1.6×10^5

Average initial bacterial concentrations for *S. aureus* were equal to 5×10^6 CFU/mL (1st week), 4.65×10^6 CFU/mL (2nd week), and 6.58×10^6 CFU/mL (3rd week).

This is an interesting observation, especially in the context of fibroblast toxicity studies (see Section 3.5). It seems that the G1, G2, G1p, and G2p granules, which contain brushite as a source of silver, do not meet the conditions of bone substitute materials releasing antibacterial agents.

Moreover, when comparing the results for granules with and without PCL, it should be noted that, in the case of granules covered with PCL, there was less inhibition of the bacterial growth, which is associated with a slower release of active substances from these types of granules, as has been seen in release studies.

4. Conclusions

In the study presented here, ciprofloxacin was loaded into composite granules containing calcium phosphates substituted with silver and gallium ions. These formulations showed a sustained release of the antibiotic and ions with antibacterial activity. During the first five hours, a slight burst release was found, while in the hours that followed, a slower, diffusion-mediated, sustained release was observed. Moreover, most of the obtained granules were able to effectively inhibit the growth of *S. aureus* and *E. coli* bacterial strains. These granules were non-toxic toward mammalian BALB/c 3T3 cells. Accordingly, composite granules have promising potential as drug carriers and bone-filling materials. The exception is granules containing Ag-DCPD, which turned out to be toxic to mammalian cells, and at the same time, granules made of it had ineffective antibacterial activity.

However, further research is necessary, and should be primarily focused on selecting the optimal granule composition in order to obtain the highest antibacterial activity while ensuring there is no toxicity to mammalian cells. It is also worth conducting research in order to select the appropriate amount of ions with antibacterial activity in relation to the amount of introduced antibiotic. In addition, further analyses should aim to use vivo models.

Supplementary Materials: The following supporting information can be downloaded at: https://www.mdpi.com/article/10.3390/coatings13030494/s1. Figure S1: FT-IR spectra of the unsubstituted calcium phosphates; Figure S2: PXRD diffractograms of the unsubstituted calcium phosphates; Figure S3: The NRU test results obtained for samples Ag-DCPD (A), G1 (B), and G2 (C) in the whole range of tested concentrations. Black stars indicate a decrease in cell viability under 70%, which classified each of these samples as cytotoxic. The rest of the tested materials did not reveal cytotoxicity in the whole range of tested dilutions; Figure S4: Cumulative release of ciprofloxacin (%)—fitting curves. A—the composite without PCL; B the composite coated with PCL.

References

1. Chen, A.F.; Wessel, C.B.; Rao, N. Staphylococcus aureus screening and decolonization in orthopedic surgery and reduction of surgical site infections. *Clin. Orthop. Relat. Res.* **2013**, *471*, 2383–2399. [CrossRef] [PubMed]
2. Cheng, L.; Li, R.; Liu, G.; Zhang, Y.; Tang, X.; Wang, J.; Liu, H.; Qin, Y. Potential antibacterial mechanism of silver nanoparticles and the optimization of orthopedic implants by advanced modification technologies. *Int. J. Nanomed.* **2018**, *13*, 3311.
3. Chae, K.; Jang, W.Y.; Park, K.; Lee, J.; Kim, H.; Lee, K.; Lee, C.K.; Lee, Y.; Lee, S.H.; Seo, J. Antibacterial infection and immune-evasive coating for orthopedic implants. *Sci. Adv.* **2020**, *6*, eabb0025. [CrossRef]
4. Jenks, P.; Laurent, M.; McQuarry, S.; Watkins, R. Clinical and economic burden of surgical site infection (SSI) and predicted financial consequences of elimination of SSI from an English hospital. *J. Hosp. Infect.* **2014**, *86*, 24–33. [CrossRef]
5. Greene, L.R. Guide to the elimination of orthopedic surgery surgical site infections: An executive summary of the Association for Professionals in Infection Control and Epidemiology elimination guide. *Am. J. Infect. Control.* **2012**, *40*, 384–386. [CrossRef] [PubMed]
6. Khalid, H.; Nafees, F.; Khaliq, M.A. Infective Organisms and their Changing Antibiotic Sensitivity Trends in Surgical Site Infection after Orthopedic Implant Surgeries. *Pak. J. Med. Health Sci.* **2018**, *12*, 1256–1258.
7. Li, B.; Webster, T.J. Bacteria antibiotic resistance: New challenges and opportunities for implant-associated orthopedic infections. *J. Orthop. Res.* **2018**, *36*, 22–32. [CrossRef] [PubMed]
8. Blondeau, J.M. Fluoroquinolones: Mechanism of action, classification, and development of resistance. *Surv. Ophthalmol.* **2004**, *49*, S73–S78. [CrossRef] [PubMed]
9. Manchon, A.; Prados-Frutos, J.C.; Rueda-Rodriguez, C.; Salinas-Goodier, C.; Alkhraisat, M.H.; Rojo, R.; Rodriguez-Gonzalez, A.; Berlanga, A.; Lopez-Cabarcos, E. Antibiotic release from calcium phosphate materials in oral and maxillofacial surgery. molecular, cellular, and pharmaceutical aspects. *Curr. Pharm. Biotechnol.* **2017**, *18*, 52–63. [CrossRef]
10. Rehman, A.; Patrick, W.M.; Lamont, I.L. Mechanisms of ciprofloxacin resistance in Pseudomonas aeruginosa: New approaches to an old problem. *J. Med. Microbiol.* **2019**, *68*, 1–10. [CrossRef]
11. Lu, M.; Liao, J.; Dong, J.; Wu, J.; Qiu, H.; Zhou, X.; Li, J.; Jiang, D.; He, T.-C.; Quan, Z. An effective treatment of experimental osteomyelitis using the antibacterial titanium/silver-containing nHP66 (nano-hydroxyapatite/polyamide-66) nanoscaffold biomaterials. *Sci. Rep.* **2016**, *6*, 39174. [CrossRef]

12. Sorinolu, A.J.; Godakhindi, V.; Siano, P.; Vivero-Escoto, J.L.; Munir, M. Influence of silver ion release on the inactivation of antibiotic-resistant bacteria using light-activated silver nanoparticles. *Mater. Adv.* **2022**, *3*, 9090–9102. [CrossRef]
13. McRee, A.E. Therapeutic review: Silver. *J. Exot. Pet Med.* **2015**, *2*, 240–244. [CrossRef]
14. Barras, F.; Aussel, L.; Ezraty, B. Silver and antibiotic, new facts to an old story. *Antibiotics* **2018**, *7*, 79. [CrossRef] [PubMed]
15. Kolmas, J.; Groszyk, E.; Kwiatkowska-Różycka, D. Substituted hydroxyapatites with antibacterial properties. *BioMed. Res. Int.* **2014**, *2014*, 178123. [CrossRef] [PubMed]
16. Best, M.G.; Cunha-Reis, C.; Ganin, A.Y.; Sousa, A.; Johnston, J.; Oliveira, A.L.; Smith, D.G.; Yiu, H.H.; Cooper, I.R. Antimicrobial properties of gallium (III)-and iron (III)-Loaded polysaccharides affecting the growth of Escherichia coli, Staphylococcus aureus, and Pseudomonas aeruginosa, in vitro. *ACS Appl. Biol. Mater.* **2020**, *3*, 7589–7597. [CrossRef]
17. Łapa, A.; Cresswell, M.; Campbell, I.; Jackson, P.; Goldmann, W.H.; Detsch, R.; Boccaccini, A.R. Gallium-and cerium-doped phosphate glasses with antibacterial properties for medical applications. *Adv. Eng. Mater.* **2020**, *22*, 1901577. [CrossRef]
18. Li, H.-K.; Rombach, I.; Zambellas, R.; Walker, A.S.; McNally, M.A.; Atkins, B.L.; Lipsky, B.A.; Hughes, H.C.; Bose, D.; Kümin, M. Oral versus intravenous antibiotics for bone and joint infection. *N. Engl. J. Med.* **2019**, *380*, 425–436. [CrossRef] [PubMed]
19. Romanò, C.L.; Scarponi, S.; Gallazzi, E.; Romanò, D.; Drago, L. Antibacterial coating of implants in orthopedics and trauma: A classification proposal in an evolving panorama. *J. Orthop. Surg. Res.* **2015**, *10*, 1–11. [CrossRef] [PubMed]
20. Dorozhkin, S.V. Bioceramics of calcium orthophosphates. *Biomaterials* **2010**, *31*, 1465–1485. [CrossRef]
21. Dorozhkin, S.V. Nanosized and nanocrystalline calcium orthophosphates. *Acta Biomater.* **2010**, *6*, 715–734. [CrossRef] [PubMed]
22. Bal, Z.; Kaito, T.; Korkusuz, F.; Yoshikawa, H. Bone regeneration with hydroxyapatite-based biomaterials. *Emergent Mater.* **2020**, *3*, 521–544. [CrossRef]
23. Bouler, J.-M.; Pilet, P.; Gauthier, O.; Verron, E. Biphasic calcium phosphate ceramics for bone reconstruction: A review of biological response. *Acta Biomater.* **2017**, *53*, 1–12. [CrossRef] [PubMed]
24. Owen, G.R.; Dard, M.; Larjava, H. Hydroxyapatite/beta-tricalcium phosphate biphasic ceramics as a regenerative material for the repair of complex bone defects. *J. Biomed. Mater. Res. Part B Appl. Biomater.* **2018**, *106*, 2493–2512. [CrossRef]
25. Schmitz, J.P.; Hollinger, J.O.; Milam, S.B. Reconstruction of bone using calcium phosphate bone cements: A critical review. *J. Oral Maxillofac. Surg.* **1999**, *57*, 1122–1126. [CrossRef]
26. Mofakhami, S.; Salahinejad, E. Biphasic calcium phosphate microspheres in biomedical applications. *J. Control. Release* **2021**, *338*, 527–536. [CrossRef]
27. Shao, R.; Quan, R.; Zhang, L.; Wei, X.; Yang, D.; Xie, S. Porous hydroxyapatite bioceramics in bone tissue engineering: Current uses and perspectives. *J. Ceram. Soc. Japan* **2015**, *123*, 17–20. [CrossRef]
28. Predoi, D.; Iconaru, S.L.; Predoi, M.H.; Buton, N. Development of novel tetracycline and ciprofloxacin loaded silver doped hydroxyapatite suspensions for biomedical applications. *Antibiotics* **2022**, *12*, 74. [CrossRef]
29. Jackson, J.; Lo, J.; Hsu, E.; Burt, H.M.; Shademani, A.; Lange, D. The combined use of gentamycin and silver nitrate in bone cement for a synergistic and extended antibiotic action against Gram-positive and Gram-negative bacteria. *Materials* **2021**, *14*, 3413. [CrossRef]
30. Wan, G.; Ruan, L.; Yin, Y.; Yang, T.; Ge, M.; Cheng, X. Effects of silver nanoparticles in combination with antibiotics on the resistant bacteria Acinetobacter baumannii. *Int. J. Nanomed.* **2016**, *11*, 3789–3800. [CrossRef]
31. Pajor, K.; Pajchel, Ł.; Zgadzaj, A.; Piotrowska, U.; Kolmas, J. Modifications of hydroxyapatite by gallium and silver ions—Physicochemical characterization, cytotoxicity, and antibacterial evaluation. *Int. J. Mol. Sci.* **2020**, *21*, 5006. [CrossRef] [PubMed]
32. *EN ISO 10993-5*; 2009 Biological Evaluation of Medical Devices—Part 5: Tests for in Vitro Cytotoxicity (ISO 10993-5:2009), Annex A Neutral Red Uptake (NRU) Cytotoxicity Test. International Organization for Standardization: Geneva, Switzerland, 2009.
33. *EN ISO 10993-12*; 2012 Biological Evaluation of Medical Devices—Part 12: Sample Preparation and Reference Materials (ISO 10993-12:2012). International Organization for Standardization: Geneva, Switzerland, 2012.
34. Sayahi, M.; Santos, J.; El-Feki, H.; Charvillat, C.; Bosc, F.; Karacan, I.; Milthorpe, B.; Drouet, C. Brushite (Ca,M)HPO$_4$, 2H$_2$O doping with bioactive ions (M = Mg^{2+}, Sr^{2+}, Zn^{2+}, Cu^{2+}, and Ag$^+$): A new path to functional biomaterials? *Mater. Today Chem.* **2020**, *16*, 10030. [CrossRef]
35. Fadeeva, I.V.; Gafurov, M.R.; Kiiaeva, I.A.; Orlinskii, S.B.; Kuznetsova, L.M.; Filippov, Y.Y.; Fomin, A.S.; Davydova, G.A.; Selezneva, I.I.; Barinov, S.M. Tricalcium phosphate ceramics doped with silver, copper, zinc and iron (III) ions in concentration of less than 0.5% for bone tissue regeneration. *BioNanoScience* **2017**, *7*, 434–438. [CrossRef]
36. Kolmas, J.; Groszyk, E.; Piotrowska, U. Nanocrystalline hydroxyapatite enriched in selenite and manganese ions: Physicochemical and antibacterial properties. *Nanoscale Res. Lett.* **2015**, *10*, 989. [CrossRef]
37. Gopi, D.; Shinyjoy, E.; Kavitha, L. Synthesis and spectral characterization of silver/magnesium co-substituted hydroxyapatite for biomedical applications. *Spectrochim. Acta Part A Mol. Biomol. Spectrosc.* **2014**, *127*, 286–291. [CrossRef]
38. Okada, M.; Furuzono, T. Hydroxylapatite nanoparticles: Fabrication methods and medical applications. *Sci. Technol. Adv. Mater.* **2012**, *13*, 064103. [CrossRef]
39. Jillavenkatesa, A.; Condrate Sr, R. The infrared and Raman spectra of β-and α-tricalcium phosphate (Ca$_3$(PO$_4$)$_2$). *Spectrosc. Lett.* **1998**, *31*, 1619–1634. [CrossRef]
40. Martínez, T.; Espanol, M.; Charvillat, C.; Marsan, O.; Ginebra, M.; Rey, C.; Sarda, S. α-tricalcium phosphate synthesis from amorphous calcium phosphate: Structural characterization and hydraulic reactivity. *J. Mater. Sci.* **2021**, *56*, 13509–13523. [CrossRef]

41. Kolmas, J.; Kaflak, A.; Zima, A.; Ślósarczyk, A. Alpha-tricalcium phosphate synthesized by two different routes: Structural and spectroscopic characterization. *Ceram. Int.* **2015**, *41*, 5727–5733. [CrossRef]

42. Boonchom, B.; Baitahe, R. Synthesis and characterization of nanocrystalline manganese pyrophosphate $Mn_2P_2O_7$. *Mater. Lett.* **2009**, *63*, 2218–2220. [CrossRef]

43. El Kady, A.M.; Mohamed, K.R.; El-Bassyouni, G.T. Fabrication, characterization and bioactivity evaluation of calcium pyrophosphate/polymeric biocomposites. *Ceram. Int.* **2009**, *35*, 2933–2942. [CrossRef]

44. dos Santos Tavares, D.; de Oliveira Castro, L.; de Almeida Soares, G.D.; Alves, G.G.; Granjeiro, J.M. Synthesis and cytotoxicity evaluation of granular magnesium substituted β-tricalcium phosphate. *J. Appl. Oral Sci.* **2013**, *21*, 37–42. [CrossRef] [PubMed]

45. Walczyk, D.; Malina, D.; Krol, M.; Pluta, K.; Sobczak-Kupiec, A. Physicochemical characterization of zinc-substituted calcium phosphates. *Bull. Mater. Sci.* **2016**, *39*, 525–535. [CrossRef]

46. Lee, D.; Kumta, P.N. Chemical synthesis and stabilization of magnesium substituted brushite. *Mater. Sci. Eng. C* **2010**, *30*, 934–943. [CrossRef]

47. Arbez, B.; Kun-Darbois, J.D.; Convert, T.; Guillaume, B.; Mercier, P.; Huber, L.; Chappard, D. Biomaterial granules used for filling bone defects constitute 3D scaffolds: Porosity, microarchitecture, and molecular composition analyzed by microCT and Raman microspectroscopy. *J. Biomed. Mater. Res. B* **2019**, *107*, 415–423. [CrossRef]

48. Szurkowska, K.; Zgadzaj, A.; Kuras, M.; Kolmas, J. Novel hybrid material based on Mg^{2+} and SiO_4^{4-} co-substituted nanohydroxyapatite, alginate and chondroitin sulfate for potential use in biomaterials engineering. *Ceram. Int.* **2018**, *44*, 18551–18559. [CrossRef]

49. Pajor, K.; Michalicha, A.; Belcarz, A.; Pajchel, L.; Zgadzaj, A.; Wojas, F.; Kolmas, J. Antibacterial and cytotoxicity evaluation of new hydroxyapatite-based granules containing silver or gallium ions with potential use as bone substitutes. *Int. J. Mol. Sci.* **2022**, *23*, 7102. [CrossRef]

50. Kurtjak, M.; Vucomanovic, M.; Krajnc, A.; Kramer, L.; Turk, B.; Suvorow, D. Designing Ga(III)-containing hydroxyapatite with antibacterial activity. *RSC Adv.* **2016**, *6*, 112839–112852. [CrossRef]

51. Cavallaro, G.; Lazzara, G.; Milioto, S.; Parisi, F.; Evtugyn, V.; Roshina, E.; Fakhrullin, R. Nanohydrogel formation within the halloysite lument for triggered and sustained release. *ACS Appl. Mater. Interface* **2018**, *10*, 8265–8273. [CrossRef]

52. Fosca, M.; Rau, J.V.; Uskokovic, V. Factors influencing the drug release from calcium phosphate cements. *Bioactive Mater.* **2022**, *7*, 341–363. [CrossRef]

53. Lisuzzo, L.; Cavallaro, G.; Milioto, S.; Lazzara, G. Halloysite nanotubes coated by chitosan for controlled release of khellin. *Polymers* **2020**, *12*, 1766. [CrossRef] [PubMed]